An orally active carbon monoxide-releasing molecule enhances beneficial gut microbial species to combat obesity in mice

Djamal Eddine Benrahla, Shruti Mohan, Matija Trickovic, Florence Anne Castelli, Ghida Alloul, Arielle Sobngwi, Rosa Abdiche, Silas Kieser, Vanessa Demontant, Elisabeth Trawinski, et al.

Redox Biology 72 (2024) 103153

Contents lists available at ScienceDirect

Redox Biology

journal homepage: www.elsevier.com/locate/redox

An orally active carbon monoxide-releasing molecule enhances beneficial gut microbial species to combat obesity in mice

Djamal Eddine Benrahla [a], Shruti Mohan [a], Matija Trickovic [b,c], Florence Anne Castelli [d], Ghida Alloul [a], Arielle Sobngwi [a], Rosa Abdiche [a], Silas Kieser [b,c], Vanessa Demontant [e], Elisabeth Trawinski [e], Céline Chollet [d], Christophe Rodriguez [a,e,f], Hiroaki Kitagishi [g], François Fenaille [d], Mirko Trajkovski [b,c], Roberto Motterlini [a,**,1], Roberta Foresti [a,*,1]

[a] University Paris-Est Créteil, INSERM, IMRB, F-94010, Créteil, France
[b] Department of Cell Physiology and Metabolism, Centre Medical Universitaire (CMU), Faculty of Medicine, University of Geneva, Geneva, Switzerland
[c] Diabetes Centre, Faculty of Medicine, University of Geneva, Geneva, Switzerland
[d] Université Paris-Saclay, CEA, INRAE, Département Médicaments et Technologies pour la Santé (DMTS), MetaboHUB, 91191 Gif-sur-Yvette, France
[e] NGS Platform, Henri Mondor Hospital, AP-HP, and IMRB Institute, University of Paris-Est-Créteil, Créteil, France
[f] Microbiology Unit, Department of Diagnostic, Prevention and Treatment of Infections, Henri Mondor Hospital, AP-HP, University of Paris-Est Créteil, Créteil, France
[g] Department of Molecular Chemistry and Biochemistry, Faculty of Science and Engineering, Doshisha University, Kyotanabe, Kyoto, 610-0321, Japan

A B S T R A C T

Carbon monoxide (CO), a gaseous signaling molecule, has shown promise in preventing body weight gain and metabolic dysfunction induced by high fat diet (HFD), but the mechanisms underlying these effects are largely unknown. An essential component in response to HFD is the gut microbiome, which is significantly altered during obesity and represents a target for developing new therapeutic interventions to fight metabolic diseases. Here, we show that CO delivered to the gut by oral administration with a CO-releasing molecule (CORM-401) accumulates in faeces and enriches a variety of microbial species that were perturbed by a HFD regimen. Notably, *Akkermansia muciniphila*, which exerts salutary metabolic effects in mice and humans, was strongly depleted by HFD but was the most abundant gut species detected after CORM-401 treatment. Analysis of bacterial transcripts revealed a restoration of microbial functional activity, with partial or full recovery of the Krebs cycle, β-oxidation, respiratory chain and glycolysis. Mice treated with CORM-401 exhibited normalization of several plasma and fecal metabolites that were disrupted by HFD and are dependent on *Akkermansia muciniphila's* metabolic activity, including indoles and tryptophan derivatives. Finally, CORM-401 treatment led to an improvement in gut morphology as well as reduction of inflammatory markers in colon and cecum and restoration of metabolic profiles in these tissues. Our findings provide therapeutic insights on the efficacy of CO as a potential prebiotic to combat obesity, identifying the gut microbiota as a crucial target for CO-mediated pharmacological activities against metabolic disorders.

1. Introduction

Carbon monoxide (CO) is a product of heme degradation by the enzyme heme oxygenase-1 (HO-1) and exerts signaling actions in mammalian organisms [1,2]. Previous evidence suggested a role of CO in diseases characterized by metabolic dysfunction. For example, a defective insulin release coincides with a reduced production of heme oxygenase-derived CO in islets of diabetic rats [3]. Likewise, hemin and heme arginate, which are both potent inducers of HO-1 gene expression and serve as substrates for endogenous CO production, were reported to alleviate adipose tissue inflammation and ameliorate insulin sensitivity and glucose metabolism [4]. Although the exact mechanism(s) by which CO affects energetic metabolism is currently unknown, mitochondria appear to be one plausible target. Recently we reported that CO liberated by CORM-401, a CO-releasing molecule that delivers CO with high efficiency in biological systems, modulates mitochondrial function and glucose metabolism in adipocytes and other cells [5,6]. We also demonstrated that oral administration of CORM-401 to mice fed a high fat diet (HFD) reduced thier body weight gain and ameliorated their metabolic profiles [6]. Treatment with CORM-401 resulted in a transient increase in blood carboxyhemoglobin (COHb), accumulation of CO in adipose tissue and uncoupling of mitochondrial respiration in adipocytes. This was followed by a switch of adipose tissue metabolism towards glycolysis and increased insulin sensitivity, highlighting one of

* Corresponding author.
** Corresponding author.
E-mail addresses: roberto.motterlini@inserm.fr (R. Motterlini), roberta.foresti@inserm.fr (R. Foresti).
[1] R.F. and R.M. equally contributed to this work.

https://doi.org/10.1016/j.redox.2024.103153
Received 6 March 2024; Received in revised form 29 March 2024; Accepted 4 April 2024
Available online 9 April 2024

the mechanisms by which CO protects against metabolic dysfunction in obesity. Since CO derived from CORM-401 will diffuse not only in blood and adipose tissue but also to other body compartments, the beneficial action of CO in obesity may depend on its interaction with multiple organs, including the microbiota population that resides in the gut.

The gut microbiota affects various aspects of host physiology, including metabolic homeostasis, tissue growth and immunity [7]. Several studies have documented that changes in microbiota composition and function contribute to various diseases in mice and humans. Accordingly, targeting the microbiota is emerging as a compelling strategy for therapeutic interventions [8] in obesity and its associated morbidities [8,9]. Diet is a key environmental factor that affects the microbiota and an unhealthy microbiome (dysbiosis), characterized by an increase in *Firmicutes* and a decline in *Bacteroidetes* phyla, has been associated with obesity [10,11]. Moreover, a lower abundance of the beneficial species *Akkermansia muciniphila* (*A. muciniphila*) from the *Verrucomicrobiota* phylum has been shown in obese humans and rodents compared to lean subjects [12]. Interestingly, administration of *A. muciniphila* reversed many metabolic dysfunctions, including adipose tissue inflammation and insulin resistance, observed in HFD fed mice and human volunteers in pre-diabetic state [13,14]. Thus, strategies that counter the decrease in *A. muciniphila* may be particularly attractive for the treatment of obesity and metabolic disorders [15].

In this study we investigated the impact of CORM-401 treatment on the gut microbiome and metabolic adaptations in mice fed a HFD regimen. We reveal that oral administration of CORM-401 to obese mice results in a high accumulation of CO in faeces, while also reshaping the microbiota profile and function towards a healthier phenotype. This effect is accompanied by normalization of plasma and faecal metabolites, such as amino acids and products of tryptophan metabolism, and glycolysis, which are altered by HFD. We demonstrate that CORM-401 stimulates a strong enrichment of *A. muciniphila* species in HFD-treated mice, suggesting that CO-based therapeutics could be used as prebiotics to counteract different pathologies characterized by dysbiosis.

2. Materials and methods

2.1. Chemicals and reagents

CORM-401 [$Mn(CO)_4\{S_2CN(CH_3)CH_2COOH)\}$] was synthesized as previously described by our group [16,17]. Stock solutions were prepared by solubilizing CORM-401 in Dulbecco phosphate buffer solution (DPBS, pH = 7.5) and stored at −20 °C until use. As shown in the chemical formula, CORM-401 consists of a manganese metal coordinated to four CO groups and to a dithiocarbamate ligand [(-S2CNMe (CH2CO2H)]. Thus, a combination of manganese sulfate (Mn_2SO_4) and N-(dithiocarboxy)sarcosine diammonium salt ($Na[S_2CN(CH_3)CH_2COONa]$) (Carbosynth, United Kingdom), representing the backbone of CORM-401, was used a negative control (indicated in the text as "MnS"). HemoCD1 was synthesized and kindly provided by Prof. Hirooaki Kitagishi [18,19]. High fat diet (60 kcal% fat, D12492i) was purchased from Research Diets (Brogaarden, Denmark) and the standard diet was obtained from ssniff Spezialdiäten GmbH (Germany). For metabolic tests, insulin (Umuline 100 UI/mL) was obtained from Lilly. Glucose, DPBS and all other reagents were obtained from Life technologies or Sigma unless otherwise specified. All analytical grade reference compounds for metabolomic analysis were from Sigma. The standard mixtures used for the external calibration of the MS instrument were from Thermo Fisher Scientific. Acetonitrile (ACN) was from SDS (Peypin, France), formic acid from Merck (France), methanol from VWR Chemicals (France) and deionized water from Biosolve chemicals (France).

2.2. Animals and experimental protocols

Eight-week-old wild-type C57BL/6JRj male mice (Janvier Labs, France) were housed (n = 5 per cage) under controlled temperature (21 °C ± 1 °C), hygrometry (60 % ± 10 %) and lighting conditions (12:12 L/D cycle). Animals were acclimatized in the animal facility for 1 week before the start of experiments. Mice were fed a standard diet (SD) or a high fat diet (HFD) and randomly assigned to 4 groups (n = 10 per group): (1) SD; (2) HFD; (3) HFD administered with CORM-401 (HFD-CO) and (4) HFD administered with the negative control (MnS). CORM-401 (30 mg/kg = 0.09 mmol/kg) and MnS (0.09 mmol/kg) were orally administered three times a week for 14 weeks as previously described [6,20]. Body weight was recorded weekly and food consumption was assessed at weeks 7 and 14. For this, food was weighed daily in the afternoon and averaged for each mouse over 24 h to determine food intake. Fecal pellets were collected prior to the beginning of the different protocols and in the last week of treatment for metabolomics and bacterial metagenomics and metatranscriptomic analysis. Mice were sacrificed at the end of 14 weeks after a 6-h fasting and 48 h after the last CORM-401 administration. Blood was collected for metabolomic and biochemical analysis. Colon and cecum were collected for measuring length and weight, respectively, before snap-freezing. Liver, epididymal white adipose tissue (eWAT), muscle and cecum content were snap-frozen in liquid nitrogen and stored at −80 °C for further analysis. All experimental procedures were approved and conducted according to institutional and INSERM guidelines.

2.3. Quantification of CO levels in blood, organs and faeces

Mice were orally administered PBS or CORM-401 (30 mg/kg) and sacrificed after 1, 3, 6, 24 and 48 h. Faeces and blood were first collected and then mice were flushed with 0.9 % saline through transcardial perfusion in order to remove all blood from organs, which were immediately snap-frozen in liquid nitrogen and stored at −80 °C. Blood carboxyhemoglobin (COHb) was determined by a spectrophotometric method previously described [21] and modified by us [22]. Briefly, blood (5 μl) collected at different time points following treatments was transferred to a sealed cuvette containing 4.5 ml tris(hydroxymethyl) aminomethane solution (20 mM) deoxygenated with sodium dithionite ($Na_2S_2O_4$) and absorbance spectra were recorded over time using a UV–Vis spectrophotometer (V-730ST JASCO, France). COHb (%) was calculated based on the reported extinction coefficients at 420 and 432 nm for mouse blood [21]. CO accumulation in faeces and tissues was assessed using the sensitive CO scavenger hemoCD1 as previously described [19]. Briefly, 10–20 mg of tissue or fecal samples were homogenized in 0.5 ml of DPBS in the presence of NaS_2O_4 (1–2 mg) and hemoCD1 (2–10 μM) was added thereafter. Samples were centrifuged at 12,000 *g* for 15 min and supernatants filtered using 0.22 μm filters. The final solutions were treated again with 1–2 mg $Na_2S_2O_4$ before absorbance spectra were recorded. The amount of CO was calculated based on the reported extinction coefficients for hemoCD1 at 422 and 434 nm and expressed over mg of tissue/faeces [19,20].

2.4. Glucose and insulin tolerance tests

Insulin sensitivity (ITT) and glucose tolerance (GTT) tests were assessed in all mice at weeks 13 and 14, respectively. Mice were first fasted for 6 h and then blood was collected from the tail to assess blood glucose using FreeStyle Optium Blood Glucose Test Strips (Abbott, France). Subsequently, glucose (1.5 g/kg) or insulin (0.3 UI/kg) solutions were administered into mice by intraperitoneal injection, and blood glucose measured at 15, 30, 60, 90, and 120 min after injection. Graphpad Prism was used to calculate the area under the curve (AUC) for blood glucose levels.

2.5. Metagenomic sequencing

Bead beating was performed as a pre-extraction step on fecal samples. DNA was then extracted with PowerFecal Pro DNA kit (938036, Qiagen) on a QIAsymphony machine (Qiagen). Genomic DNA libraries were constructed using the Nextera XT kit (Illumina) and pair-end sequenced (2 x 150 bp) with the NextSeq 500/550 high output kit v2.5 (300 cycles) at the genomic platform of Henri Mondor Hospital.

2.6. Metatranscriptomics sequencing

Bacterial RNA was extracted from fecal samples using QIAsymphony PowerFecal Pro DNA kit (938036, Qiagen). Metatranscriptomics libraries were prepared using Illumina TruSeq RNA Sample Preparation Kit v2. For this, purification of mRNA is performed using paramagnetic beads after depleting ribosomal (r)RNA transcripts from 0.1 to 1 μg of total RNA. Following purification, the RNA is fragmented and followed by first strand cDNA reverse transcription from the cleaved RNA fragments using reverse transcriptase and random primers. Second-strand cDNA synthesis was performed using DNA Polymerase I and RNase H. The 3′ Ends of double strands (ds) cDNA were adenylated by the addition of a single 'A' base. Multiple indexing adapters were added to the ends of the ds cDNA. The indexed DNA fragments are purified and enriched with PCR. The final cDNA library was normalized and pooled then sequenced on a NovaSeq 6000 system (Illumina) following a 300-cycle paired-end protocol.

2.7. Microbiome analysis

Metagenomic reads were quality-controlled using the 'QC' module from atlas v2 (https://doi.org/10.1186/s12859-020-03585-4). In brief, employing tools from the BBmap suite v37.78 (referenced at https://www.osti.gov/biblio/1241166), reads were quality-trimmed, and contaminants from the mouse genome were removed. Bacterial species abundances were determined using the 'quantify_genomes' module from atlas v2, utilizing the CMMG mouse microbiota genome catalog (https://doi.org/10.1371/journal.pcbi.1009947) as a reference. For this purpose, sequencing reads were aligned to the reference genomes using the minimap2 aligner (https://doi.org/10.1093/bioinformatics/bty191). The coverage of each representative genome was calculated using the 'pileup' tool from the BBmap suite, with the physical coverage option enabled, folowed by centered log2 ratio transformation. The relative abundance of KEGG modules was inferred from the annotation of CMMG genomes as the sum of the relative abundances of all species annotated with that module. The metatranscriptomics analysis followed a similar procedure as the metagenomic data, with the addition that rDNA sequences were also filtered out.

2.8. Fecal and plasma metabolomics profiling

Plasma and faecal samples were collected and metabolomics profiling was performed using an untargeted protocol for liquid chromatography coupled to high-resolution mass spectrometry following procedures previously described [23,24] (see details in the Supplementary Material).

2.9. Study approval

All animal experiments reported in this manuscript were approved by the Institutional Animal Ethics Committee of the Mondor Institute for Biomedical Research (IMRB). All animals received care according to the institutional guidelines of INSERM and the University Paris Est Creteil.

3. Data

Data of shotgun metagenome sequencing, faecal and plasma metabolites are available as Excel tables in the Supplementary Data Files S1, S2 and S3, respectively.

3.1. Statistical analysis

Statistical analyses were performed using Graph Prism version 9. All data are expressed as mean values ± SEM. Analyses were performed using either a two-tailed Student's *t*-test, a one-way or two-way ANOVA with Bonferroni test multiple comparisons. For non-parametric data, the Wilcoxon signed-rank test was used. Spearman tests were used to assess the significance of the correlations between bacterial species and metabolic/physiological parameters. In all cases, $P < 0.05$ was considered significant.

4. Results

4.1. CO reduces body weight gain and improves glucose metabolism in mice fed a HFD

C57BL/6 male mice fed obesogenic HFD (60 % fat) for 14 weeks were treated by oral gavage with either CORM-401 or MnS, the backbone of CORM-401 that does not contain CO and was used as negative control. CORM-401 markedly attenuated HFD-induced obesity as evidenced by a reduced body weight gain, which was very similar to that of mice under a standard diet (SD) (Fig. 1A and B; Supplementary Figure S1A), confirming previously reported data [6,20]. Notably, the increase in body weight under HFD was not affected by MnS administration, implicating CO as the main responsible for the beneficial effects mediated by CORM-401 (Fig. 1A and B; Supplementary Figure S1A). As already shown [6], food intake was similar in all groups (Supplementary Figure S1B), excluding the possibility that CORM-401 affects weight gain due to changes in eating habits. Mice fed a HFD exhibited an increase in fasting glycemia (Fig. 1C), glucose intolerance and insulin resistance (Supplementary Figure S1C to S1F). Notably, CORM-401 treatment improved these parameters towards levels observed in SD mice. MnS also induced some amelioration of glucose metabolism and insulin sensitivity, although to a much lesser extent than the active CORM-401. Plasma lactate, which declined in mice under HFD, was restored to normal values by CORM-401 (Fig. 1D). Suppression of weight gain by CORM-401 was accompanied by an overall normalization of organs appearance. Specifically, after the 14-week HFD regime, mice developed a fatty liver (Supplementary Figure S1G), skeletal muscle atrophy accompanied by surrounding fat deposition (Supplementary Figure S1H), as well as enlargement and whitening of brown adipose tissue (Supplementary Figure S1I), which were all prevented by CORM-401. Altogether, these results confirm the anti-obesogenic action of CORM-401 with profound improvements in body metabolism and prevention of the anatomical and functional deleterious effects induced by HFD.

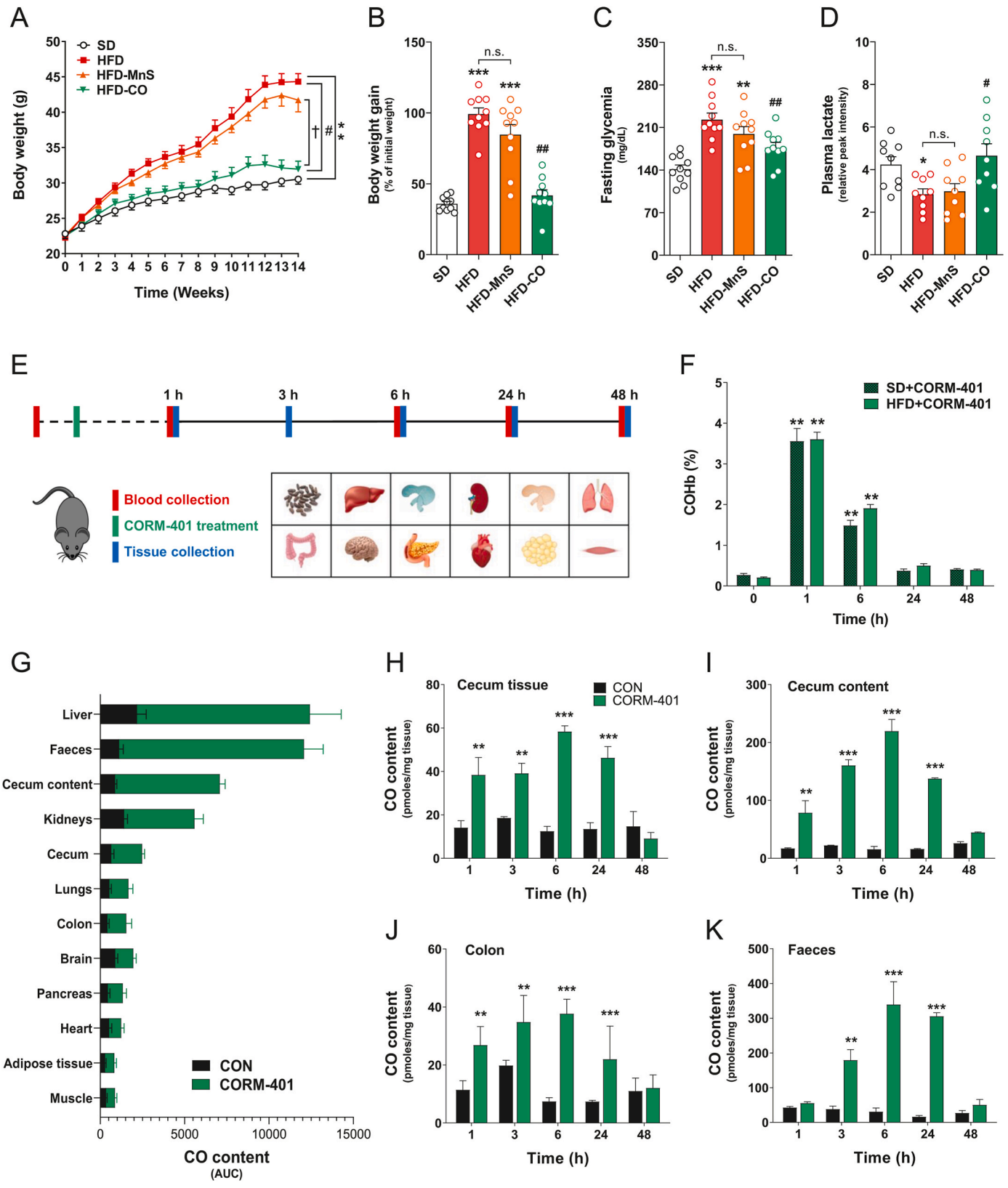

(caption on next page)

Fig. 1. CO delivered by CORM-401 to different body compartments prevents body weight gain and metabolic dysfunction in mice on HFD. Mice were maintained for 14 weeks either on a standard (SD), high fat diet (HFD), HFD plus CORM-401 (HFD-CO) or HFD plus the negative control MnS (HFD-MnS). CORM-401 (0.09 mmol/kg) or MnS (0.09 mmol/kg) was administered orally three times a week. (**A**) Body weight of animals in the four groups studied as recorded on a weekly basis (n = 10). (**B**) Body weight gain as percentage of the initial weight. (**C**) Fasting glycemia measured at week 13. (**D**) Plasma lactate levels detected by untargeted metabolomics at week 14. (**E**) Experimental design for the quantification of CO in blood and tissues. Blood was collected at different times after a single administration of CORM-401 in SD or HFD fed mice. Tissues, cecum content and faeces were collected at 1, 3, 6, 24 and 48 h after a single treatment with CORM-401 or DPBS (CON) in 8-week old mice (n = 3–5). (**F**) Blood carboxyhemoglobin (COHb) levels before and after oral gavage with CORM-401. (**G**) Total CO content in organs and faeces calculated from the area under the curve (AUC) obtained over a 48 h period following treatment with CORM-401 (green) versus untreated control (CON) mice (black). (**H–K**) Time course of CO accumulation in cecum tissue, cecum content, colon and faeces over time. Data represent the mean ± SEM. $^{*}P < 0.05$, $^{**}P < 0.01$, $^{***}P < 0.001$, vs. control group (CON), $^{\#}P < 0.05$ and $^{\#\#}P < 0.01$ vs. HFD group. n.s., non-significant. Student's *t*-test, one-way or two-way ANOVA with Bonferroni test for multiple comparisons were used. (For interpretation of the references to color in this figure legend, the reader is referred to the Web version of this article)

4.2. Administration of CORM-401 elicits a time-dependent distribution of CO in organs and different compartments of the mouse body

Administration of CORM-401 to mice has been previously shown to result in temporal increases in blood carboxyhemoglobin (COHb) levels and accumulation of CO in the adipose tissue [6]. Due to the pharmacokinetic properties of the compound and the presence of several CO-binding targets in organs/tissues, we assumed that after treatment, CO liberated by CORM-401 will also distribute in different body compartments [20]. We therefore examined CO accumulation over a time course of 48 h in blood, major tissues and organs of mice receiving CORM-401 (Fig. 1E). We measured CO spectrophotometrically using the sensitive CO scavenger hemoCD), which extracts and avidly traps CO from homogenized tissues with extremely high affinity [6,20,25]. We found a significant and similar increase in COHb in SD and HFD mice treated with CORM-401 after 1 h, which decreased thereafter to control levels by 24 and 48 h (Fig. 1F). After measuring CO content in organs, faeces and tissues over time, we calculated the area under the curve to determine the distribution of CO in different body compartments. As shown in Fig. 1G, liver and faeces displayed the highest CO levels, followed by the cecum content and the kidney. The results for the liver and kidney are consistent with their direct involvement in detoxification and elimination of pharmacological substances. The high CO levels in the cecum content and in faeces indicate the transit of CORM-401 and CO from the stomach to lower parts of the intestine before excretion. The maximal amount of CO measured in the cecum content (approx. 200 pmol/mg) and faeces (approx. 300 pmol/mg) was accompanied to a lesser extent by a significant increase in CO also in cecum and colon tissues (Fig. 1H, I, 1J, 1K). In contrast to blood, where COHb levels reached a maximum within 1 h (Fig. 1F), CO accumulation in the cecum content, faeces, colon and cecum tissue peaked at 3–6 h after CORM-401 administration. In addition, CO levels in these compartments were still high at 24 h and returned to normal values by 48 h, indicating that the dynamics of CO binding to hemoglobin are very different from the binding of CO to targets in organs and tissues. These results provide a comprehensive view of the pharmacokinetics of CORM-401 *in vivo*, highlighting that CO partially distributes to blood for a short period of time, while accumulating and lingering in specific organs over a period of 48 h after CORM-401 treatment.

4.3. CO attenuates gut microbiota dysbiosis during HFD-induced obesity

The results showing high CO levels in faeces after CORM-401 administration indicates that CO reaches the gut and that the microbiota could be implicated in the beneficial effects of CO during obesity. We thus investigated the composition of the microbiota by shotgun metagenomics analysis in faeces collected at the end of the 14-week protocols. Predictably, the microbiota profile of animals fed HFD was completely different from that of animals under SD (Fig. 2A) [26]. Moreover, the Principal Coordinate Analysis (PCoA) showed that the microbiota of mice receiving HFD + CORM-401 separated from that of animals on HFD or HFD + MnS (Fig. 2B). As reported previoulsy [10,11], we also found that under HFD the relative abundance of *Firmicutes* was markedly increased, while the *Bacteroidota* phylum was decreased, raising the *Firmicutes/Bacteroidota* ratio to ~12 from a value of ~1 in SD (Fig. 2C and D). CORM-401 partially reduced the *Firmicutes/Bacteroidota* ratio compared to HFD alone. A similar trend was observed in MnS-treated mice, however without reaching statistical significance. In addition, CORM-401/CO specifically enriched the abundance of the *Actinobacteriota*, *Desulfobacterota* and, most strikingly, the *Verrucomicrobiota* phyla (Fig. 2C and E). Metatranscriptomics analysis corroborated these findings, emphasizing a distinct transcription of bacteria species in the HFD-CO group compared to HFD and HFD-MnS (Supplementary Figure S2A, S2B, S2C).

The heatmap presented in Supplementary Figure S2D reveals 160 species (full list in accompanying Data File S1 - Excel file) that were significantly different by their transcription between HFD and HFD-CO. Some of the identified bacterial species, such as *Lactococcus lactis*, *Bifidobacterium longum* and *A. muciniphila*, are well-known, while all species containing the MGG in the name were newly uncovered using our recently developed CMMG catalogue [27,27], which achieves a coverage of the mouse gut microbiome exceeding 90 % [28]. Four patterns could be delineated from the heatmap: 1) bacterial species such as *Roseburia MGG22730*, *Acetatifactor MGG03638* or *Acetatifactor MGG02576* were low in SD, increased in HFD and HFD-MnS and were restored to near basal levels in the HFD-CO group; 2) abundant species in SD, such as *MGG05653*, *MGG05653* and *Eubacterium I MGG47456* were decreased by HFD and HFD-MnS but highly depleted in HFD-CO; 3) abundant species in SD were depleted in all the HFD groups and; 4) species that were low in SD and decreased in HFD and HFD-MnS were instead highly enriched only in HFD-CO. This fourth pattern included *A. muciniphila_B* and the unknown *NM07-P-09 sp004793925* and *CAG-594 MGG3232398* species. The Linear Discriminant Analysis (LDA) scores obtained using a cut-off of 2.5 shows the 32 bacterial clades that were significantly enriched in HFD-CO compared to HFD (Supplementary Figure S2E), including the *Rikenellaceae*, *Akkermansiaceae*, *Tannerellaceae* families and 4 unknown species (*1XD42-69MGG19677*, *UBA3282 MGG31768*, *Lawsonibacter MGG21846* and *Anaerosaccharriohilus MGG19285*). Together, our findings demonstrate that CORM-401 stimulates profound changes in microbiota composition in mice on HFD, suggesting that gut microbiome adaptations induced by CO may actively contribute to the beneficial action of this gas on weight gain and metabolic dysfunction during obesity.

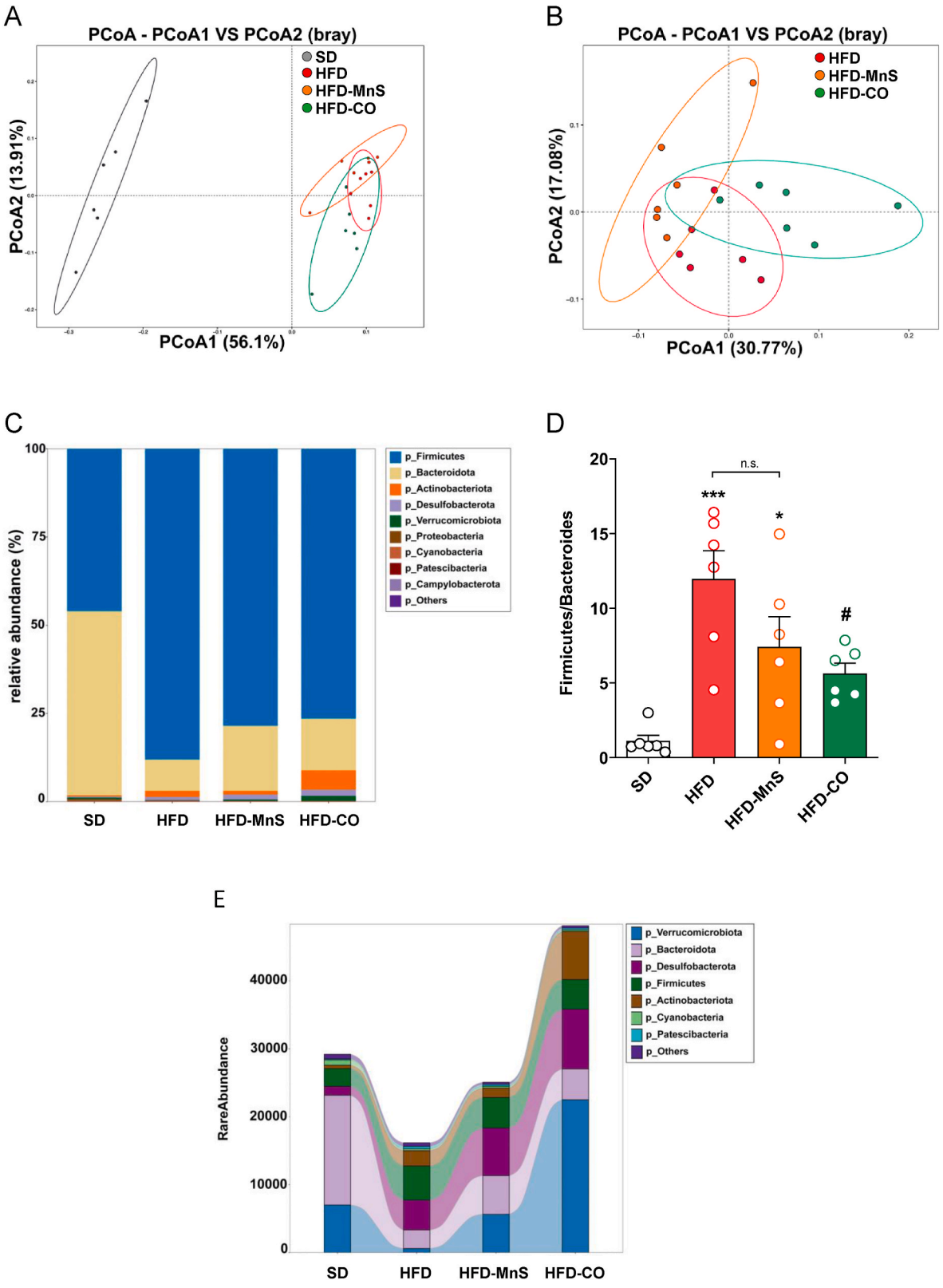

Fig. 2. CORM-401 modulates the gut microbiota composition during HFD-induced obesity. Metagenomics analysis of bacterial DNA extracted from fecal samples at week 14. (**A-B**) Principal Coordinate Analysis (Bray-Curtis distance method) plots of gut microbiota analyzed in fecal samples collected from mice under SD, HFD, HFD + MnS or HFD + CORM-401 (HFD-CO) after the 14 weeks protocol (n = 6). The plots show a clear clustering of bacterial species between SD and HFD groups (**A**) and a separation between HFD and HFD-CO (**B**). (**C**) Stacked taxonomic bar plots at the phylum level (top 10 phyla) in fecal samples from the four groups. The Metagenome-Atlas was used for annotation, the MicrobiotaProcess package was used for graphs generation. (**D**) The *Firmicutes/Bacteroidetes* ratio is significantly increased in HFD vs. SD and markedly diminished in HFD-CO. (**E**) Rare abundance of bacterial phyla in the four groups calculated from the total number of sequence reads (MicrobiotaProcess). Data represent the mean ± SEM. $^{*}P < 0.05$, $^{***}P < 0.001$, vs. SD, $^{\#}P < 0.05$ vs. HFD group. n.s., non-significant. One-way ANOVA with Bonferroni test for multiple comparisons was used.

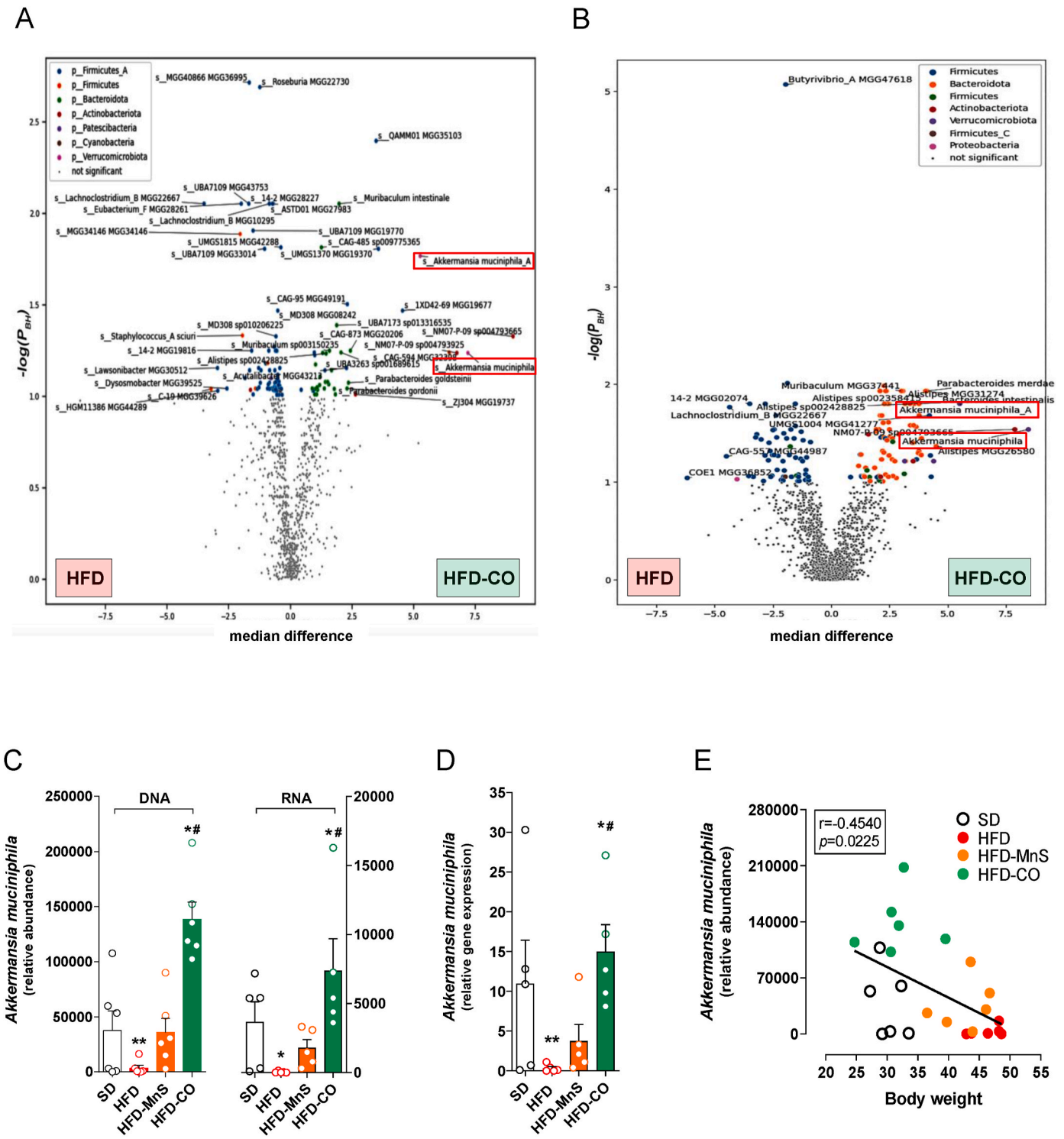

Fig. 3. CORM-401 enriches the abundance of the beneficial bacteria *A. muciniphila*. Volcano plots showing the differences of gut microbiota species at metagenomics (**A**) and metatrascriptomics (**B**) levels, respectively, in HFD vs. HFD-COs. The dot colour corresponds to the different bacterial phyla as reported on the top left hand side of the square and denotes significantly enriched species in HFD or HFD-CO. Grey dots represent non-significant species. (**C**) DNA and RNA relative counts of *A. muciniphila* species at week 14 in fecal samples from animals fed SD, HFD, HFD-MnS and HFD-CO (n = 5–6). (**D**) Relative gene abundance of *A. muciniphila* confirmed by qPCR in the same samples (n = 3). (**E**) Spearman test to assess a significant correlation between *A. muciniphila* relative abundance and body weight in the 4 groups. The Spearman coefficient (*r*) and *p* values are reported. One-way ANOVA with Bonferroni test for multiple comparisons between groups was used. Data represent the mean ± SEM. $^{*}P < 0.05$ and $^{**}P < 0.01$ vs. SD, $^{\#}P < 0.05$ vs. HFD group. (For interpretation of the references to color in this figure legend, the reader is referred to the Web version of this article.)

4.4. Akkermansia muciniphila is enriched in the gut microbiota of CO-treated mice

Metagenomic analysis of the microbiota composition between HFD and HFD-CO groups pointed to several species enriched by CORM-401 that belong to the *Bacteroidota* phylum (Fig. 3A, green dots), and a predominance of *Firmicutes* in microbiota of HFD-fed mice (blue and orange dots). Several bacteria from the *Bacteroidota* phylum in HFD-CO were identified by a code from the CMMG catalog only and are uncharacterized species. The metagenomics data (Fig. 3A) perfectly matched the metatranscriptomics analysis (Fig. 3B), indicating that changes in bacterial composition corresponded to the function of the bacterial populations. These data demonstrate that the high abundance of *Firmicutes* activity in the HFD group was shifted by CORM-401 to richness in *Bacteroidota*, followed by the *Firmicutes*, *Actinobacteriota* and *Verrucomicrobiota* phyla.

Metagenomics and metatranscriptomics comparisons between HFD and HFD-MnS suggested certain changes in the metagenomes (Supplementary Figure S3A), albeit without significant differences at the functional level (Supplementary Figure S3B). Similarly to the differences between microbiota from HFD and HFD-CO mice, the volcano plots comparing HFD-MnS and HFD-CO showed that the major differences between the groups were due to an abundance of *Firmicutes* in HFD-MnS and a more varied functional activity, with very few *Firmicutes*, in HFD-CO (Supplementary Figure S3C and S3D). Species that were functionally active in HFD-CO included *NM07-P-09 sp004793665* and *NM07-P-09 sp004793925* from the *Actinobacteroidota* phylum and *UBA2866 MGG42364* from the poorly explored *Patescibacteria*, which was shown to be increased in under-weight individuals [27] (Supplementary Figure S3D, Data File S1).

Interestingly, CO markedly enriched the abundance of *Akkermansia muciniphila (A. muciniphila)* and counteracted the profound suppressive effect of HFD on this species as identified in metagenomic and metatranscriptomic analyses (Fig. 3C) and confirmed by qPCR (Fig. 3D). *A. muciniphila* is an essential bacterium that protects against obesity and metabolic dysfunction and is investigated as a probiotic to protect against microbiota dysbiosis [15]. Indeed, our results showed that the relative abundance of the species *A. muciniphila, A. muciniphila_A*, *A. muciniphila_B* and *A. sp001580195* were negatively correlated with body weight in the four groups (Fig. 3E, Supplementary Figure S4A). Notably, the HFD-CO group showed the lowest body weight in association with the highest abundance of these species, whereas the opposite was true for the HFD groups. There was no significant correlation of these species with glycemia or ITT (Supplementary Figure S4B and 4C). We also found that the abundance of *Acetatifactor MGG29155* and *MGG47238*, *Adlercreutzia mucosicola*, *Enterocloster aldenensis*, *Lachnoclostridium B*, *Lactococcus lactis*, *Lawsonibacter MGG48410*, *Roseburia MGG22730* and *UBA9475MGG00498* species was positively correlated with body weight. Conversely, we observed a negative correlation between the body weight and abundance of *Muribaculum intestinale*, *Prevotella* sp*002298815* and *UBA3263 sp001689615* species (Supplementary Figure S4A). Again, the strong abundance of these bacterial species in the HFD-CO group was associated to a low body weight. Interestingly, the abundance of most of the bacterial species mentioned above also correlated with fasting glycemia (Supplementary Figure S4B) and ITT profiles (Supplementary Figure S4C).

We then searched in the literature whether the top 21 species significantly different between HFD and HFD-CO were already known in mice and had any relevance in the context of obesity in humans (Supplementary Table S1). We found that the abundance of *Acetatifactor*, *Adlercreutzia*, *Akkermansia*, *Alistipes*, *Lactococcus*, *Lahnoclostridium*, *Ruminococcus* and *Roseburia* species was markedly altered (increased or decreased) in obesity, in line with similar microbiota changes of these eight species observed in the HFD group of the present study. Importantly, these species were restored by CORM-401 to levels found in SD and are associated with the lean phenotype published in the literature (Supplementary Table S1).

4.5. CO stimulates the Krebs cycle and β-oxidation in gut microbiota

We next focused on the metatranscriptomics data to explore whether CO affected functional pathways in gut bacteria. We identified 37 pathways that were significantly different between HFD and HFD-CO (Fig. 4A), many of them linked to metabolism. Specifically, CORM-401 enhanced the citrate cycle (Krebs cycle) compared to HFD (Figs. 4B) and 70 bacterial species, with a predominance of the *Akkermansiaceae* family from the *Verrucomicrobiota* phylum, contributed to this pathway (Fig. 4C). We also observed that β-oxidation, which degrades fatty acids for conversion into acetyl-CoA used in the Krebs cycle, was suppressed in HFD mice but partially recovered by CORM-401 (Fig. 4D). In this case, 146 species contributed to this pathway with a strong abundance of the *Muribaculaceae* and *Rickenellaceae* families from the *Bacteroidota* phylum (Fig. 4E). The reductive citrate cycle was also enhanced in HFD-CO compared with HFD (Supplementary Figure S5A), which was again due to contribution by the *Akkermansiaceae*, but also the *Tannerellaceae* family from the *Bacteroidota* phylum (Supplementary Figure S5B). Concomitantly, the pathways of: 1) cytochrome bd ubiquinol oxidase, the terminal oxidase in the membrane respiratory chains of bacteria (Supplementary Figure S5C); 2) coenzyme A biosynthesis, which is important in fatty acids and pyruvate oxidation for entrance of acetylCoA into the Krebs cycle (Supplementary Figure S5D) and; 3) adenine ribonucleotide biosynthesis (Supplementary Figure S5E), were mostly restored to SD levels in the HFD-CO group. In addition, glycolysis was similarly recovered by CO to basal levels after a marked decline caused by HFD (see Fig. 7G below). Other key pathways activated by HFD but reduced to basal activity by CO were: 1) the V/A-type ATPase (Supplementary Figure S5F), a protein that functions as ATP hydrolysis-driven proton pump [29] and attributed to the function of 643 bacterial species (Supplementary Figure S5G), and 2) phosphatidylcholine biosynthesis (Supplementary Figure S5H), responsible for the formation of membrane phospholipids [30] and due to the contribution of 71 species, with a predominance of the *Bacteroidaceae* family from *Bacteroidota* (Supplementary Figure S5I).

These data indicate that changes in microbiota composition induced by CORM-401 result in profound modifications of microbial metabolic pathways, with a recovery of major functions related to fatty acid oxidation, Krebs cycle, bacterial respiration and glycolysis that were disrupted by the HFD regimen.

4.6. CO restores amino acids homeostasis and tryptophan metabolism in HFD-induced obesity

To gain further insight into the effects of CORM-401 on microbiota composition and function, untargeted metabolomics analyses of fecal and plasma samples were performed by liquid chromatography coupled to high-resolution mass spectrometry using a combination of two complementary chromatographic methods (see Supplementary Material). Under these conditions, we identified and robustly monitored 209 and 263 annotated metabolites in faeces and plasma, respectively (Data Files S2 and S3). Partial Least Squares Discriminant Analysis (PLS-DA) score

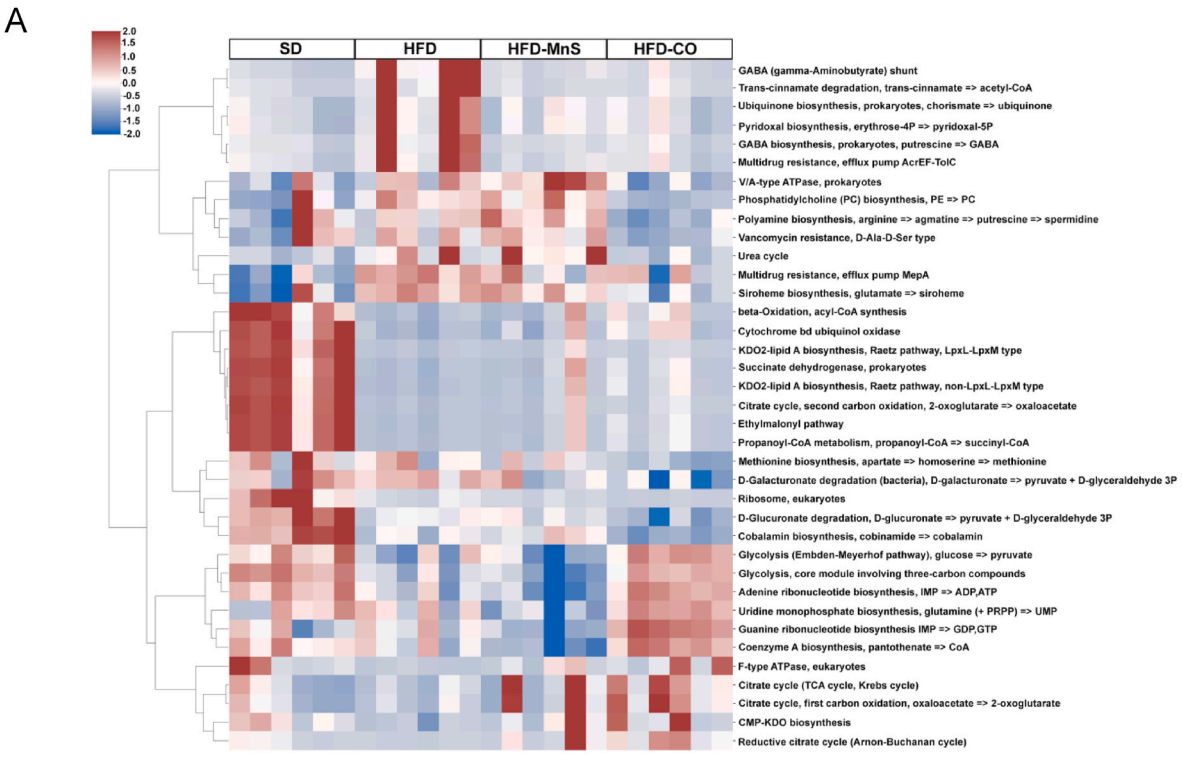

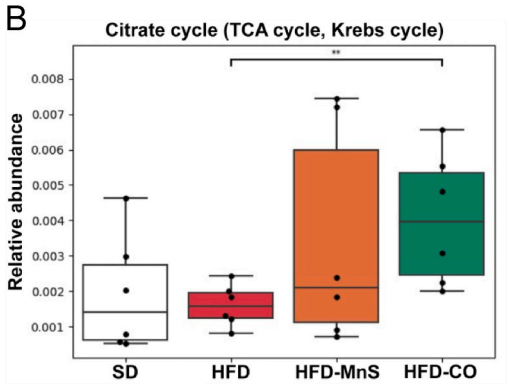

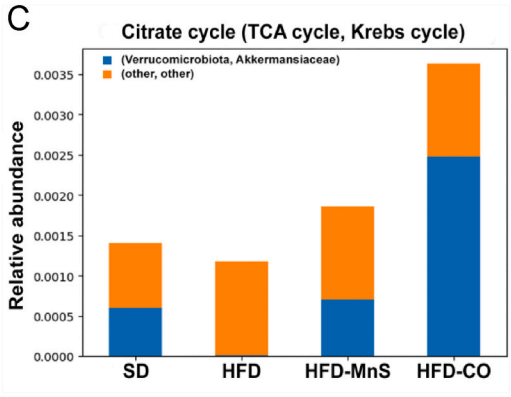

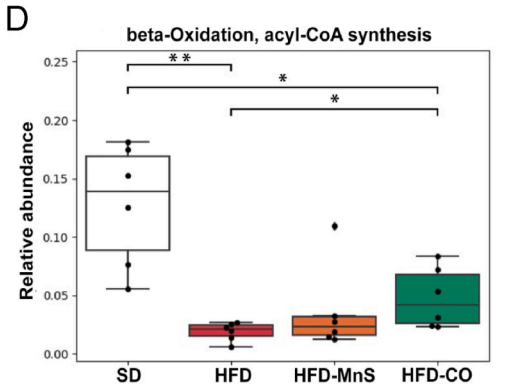

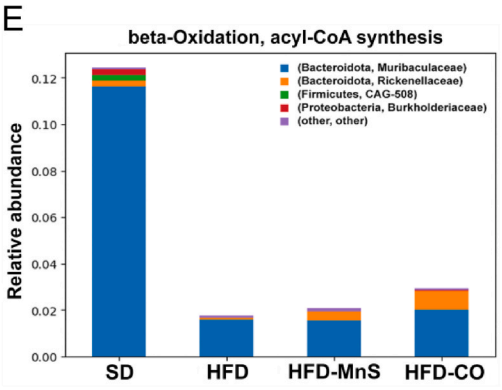

(caption on next page)

Fig. 4. CORM-401 alters selective metabolic pathways in gut microbiota during HFD. Functional analysis of the abundance of KEGG modules of gut microbiota's metabolic pathways inferred from annotation of CMMG genome from metatranscriptomic sequencing data of fecal samples from mice under SD, HFD, HFD-MnS and HFD-CO (n = 6). (**A**) Heatmap of the predictive metabolic pathways that were significantly different ($P < 0.05$) between HFD and HFD-CO. The abundance profiles were transformed into Z scores (scale shown in color bar) computed from the relative abundances of the selected metabolic pathways across different groups. (**B–C**) Relative abundance of the citrate cycle and the microbiota phyla and families, respectively, contributing to the enrichment of this pathway. (**D-E**) Relative abundance of the beta-oxidation pathway and the microbiota phyla and families, respectively, contributing to the enrichment of this pathway. The results show that in HFD-CO the *Akkermansiaceae* family from the *Verrucomicrobiota* phylum promotes the enrichment of the citrate cycle pathway, while the increase in the beta-oxidation pathway is ascribable to a great extent to the *Rickenellaceae* and a small increase in the *Muribaculaceae* families from the *Bacteroidota* phylum. Box plots were analyzed by Wilcoxon non parametric test. $^{*}P < 0.05$ and $^{**}P < 0.01$ between two groups. (For interpretation of the references to color in this figure legend, the reader is referred to the Web version of this article.)

plots showed a clear clustering of fecal metabolites detected in the positive (Fig. 5A) and negative (Fig. 5B) ion conditions between the HFD and HFD-CO groups. The heatmap in Fig. 5C reveals the 30 top metabolites significantly changed between the two groups and these included 21 amino acids or compounds from amino acid metabolism that were low in SD, increased by HFD and restored to normal levels by CO. The only exception was aspartic acid displaying low levels in SD and HFD but highly increased in HFD-CO. In addition, four fatty acids were affected by CO, followed by a miscellaneous group of substances. Fecal metabolites detected under positive and negative ion conditions were also different between SD and HFD-CO (Supplementary Figure S6A), or between HFD-CO and HFD-MnS (Supplementary Figure S6B), but to a lesser extent between HFD vs. HFD-MnS (Supplementary Figure S6A). Among the amino acids increased by HFD and normalized by CO in faeces (Data File S2) were the branched-chain amino acids (BCAAs) isoleucine/leucine (Fig. 6A), the aromatic amino acid tyrosine (Fig. 6B), which levels have been reported to be higher in obese individuals and represent a signature of insulin resistance [31,32], and betaine (Fig. 6C). Tryptophan (Fig. 6D), arginine (Fig. 6E) and asparagine (Fig. 6F) followed a similar trend. Importantly, integrative analysis of our datasets (MicrobiomeAnalyst) showed that the changes in faecal tryptophan were significantly associated with the enrichment of *A. muciniphila* in HFD-CO (Supplementary Figure S7F).

Plasma metabolites were also strongly modified by CO treatment, as reported in Supplementary Figure S7A to S7D, showing the PLS-DA score plots comparing the different groups after metabolomics analysis in both positive and negative ion modes. The heatmap in Supplementary Figure S7E depicts the 37 top metabolites significantly changed between HFD and HFD-CO, including 12 amino acid metabolites or derivatives that were depleted by HFD and HFD-MnS but restored in HFD-CO, substances from carbohydrate metabolism (phosphoenolpyruvic acid, glucose) that were increased by HFD and restored in HFD-CO, and metabolites of lipid metabolism, that were either increased (β-hydrolauric acid) or decreased (methylcrotonyl glycine) by HFD and recovered by CO. Notably, levels of 4-hydroxy indole (Fig. 6G), 5-hydroxy indole and indole propionic acid (Data File S3), which are derived from microbial tryptophan metabolism and absorbed by the host, were markedly diminished in HFD and normalized by CO. Similarly, plasma levels of cholic acid (Fig. 6H) and deoxycholic acid (Data File S3), two important endocrine molecules that facilitate the absorption of fats and regulate numerous metabolic processes [33], were decreased in HFD-fed mice and almost completely restored after CORM-401 treatment. On the contrary, the uremic toxin guanidinosuccinic acid [34,35] was enhanced in plasma of HFD and HFD-MnS mice and reduced to control levels by CO (Fig. 6I).

The decrease in plasma amino acids metabolites in HFD mice indicates an inability of the host to use amino acids for normal metabolic activities, resulting in accumulation of amino acids in faeces, which was counteracted by CO treatment. Excessive fecal amino acids in HFD may represent a burden to gut microbiota that would attempt to metabolize them, explaining the enhanced urea cycle in bacteria (Fig. 6J), mainly due to the *Oscillospiraceae* family of *Firmicutes* (Fig. 6K), which eliminates ammonia originating from degradation of amino acids. Furthermore, these results depict a mirroring scenario, where the rise in fecal tryptophan induced by HFD was accompanied by a decline in tryptophan-derived indoles in plasma, indicating that tryptophan was not metabolized by the altered microbiota population of the HFD group and that indoles were not available for absorption by the intestinal epithelium. Conversely, the normalization of fecal tryptophan with concomitant rescue of plasmatic indoles in HFD-CO reveals that the reshaping of the microbiota composition by CO reestablished their capacity to metabolize tryptophan, an effect attributed to the enrichment of *A. muciniphila* species in HFD mice receiving CORM-401.

4.7. Alteration of the glycolytic pathway induced by obesity is normalized by CO

Given the changes induced by CO on the microbiota profiles, we examined the gut for anatomical features and expression of genes that could indicate how this tissue adapted to CORM-401 treatment. First we focused on the colon and using pimonidazole staining we observed that HFD caused a hypoxic environment, which was normalized by CO (Fig. 7A and B). Colon length was also significantly reduced in HFD but CO did not reverse this effect (Supplementary Figure S8A and S8B). In line with low level of inflammation in the gut, HFD increased the expression of toll-like receptors (TLR-9 and TLR-11), which was prevented by CO (Supplementary Figure S8C). We also measured the expression of hypoxia inducible factors and found that HIF-1α was depressed (Fig. 7C) while HIF-2α was increased in all the HFD groups compared to SD (Fig. 7D). Increased hypoxia in the colon of HFD mice was accompanied by a significant increase in glucose transporters GLUT4 and SGLT1, a decrease in hexokinase2 (upper glycolysis) and an increase in pyruvate kinase and lactate dehydrogenase (lower glycolysis) expression (Fig. 7E); treatment with CORM-401 markedly reversed these changes to levels measured in SD. Interestingly, faecal lactate levels were enhanced by HFD and normalized by CO (Fig. 7F). In contrast to increased glycolysis in the colon tissue, the glycolytic pathway in the gut microbiota was profoundly inhibited by HFD but again recovered in HFD-CO (Fig. 7G), with 1412 bacterial species contributing to this effect (Fig. 7H). These included *Atopobiaceae* and *Erysipelotrichaceae* families from the *Actinobacteriota* and *Firmicutes* phyla, respectively. Interestingly, the restoration of the microbial glycolysis pathway by CO was not due to a normalization of bacterial composition observed in SD, but rather due to enrichment of several alternative microbial species that are capable of maintaining glycolysis in HFD-CO compared to HFD alone.

The cecum of HFD fed mice showed reduced weight (Supplementary Figure S8D and 8E) and low grade inflammation (Supplementary Figure S8F) that were both reversed by CO. At least 24 bacterial species were strongly correlated to the changes in cecum weight, with the *A. muciniphila A* (Supplementary Figure S8G), *Muribaculum intestinale* and *Prevotella* sp*002298815* (Supplementary Figure S8H) species positively correlated, while the unknown *Acetatifactor MGG29155*, *Acetatifactor MGG47238*, *UBA9475 MGG00498* as well as *Adlercreutzia mucosicola* and *Lactococcus Lactis* negatively correlated (Supplementary Figure S8H).

These findings highlight that CO affects the colon and cecum tissues that are in strict contact with the microbiota, inducing an amelioration of gut anatomy disrupted by HFD and affecting the tissue metabolic (glycolysis) and inflammation responses that are altered in obesity. We

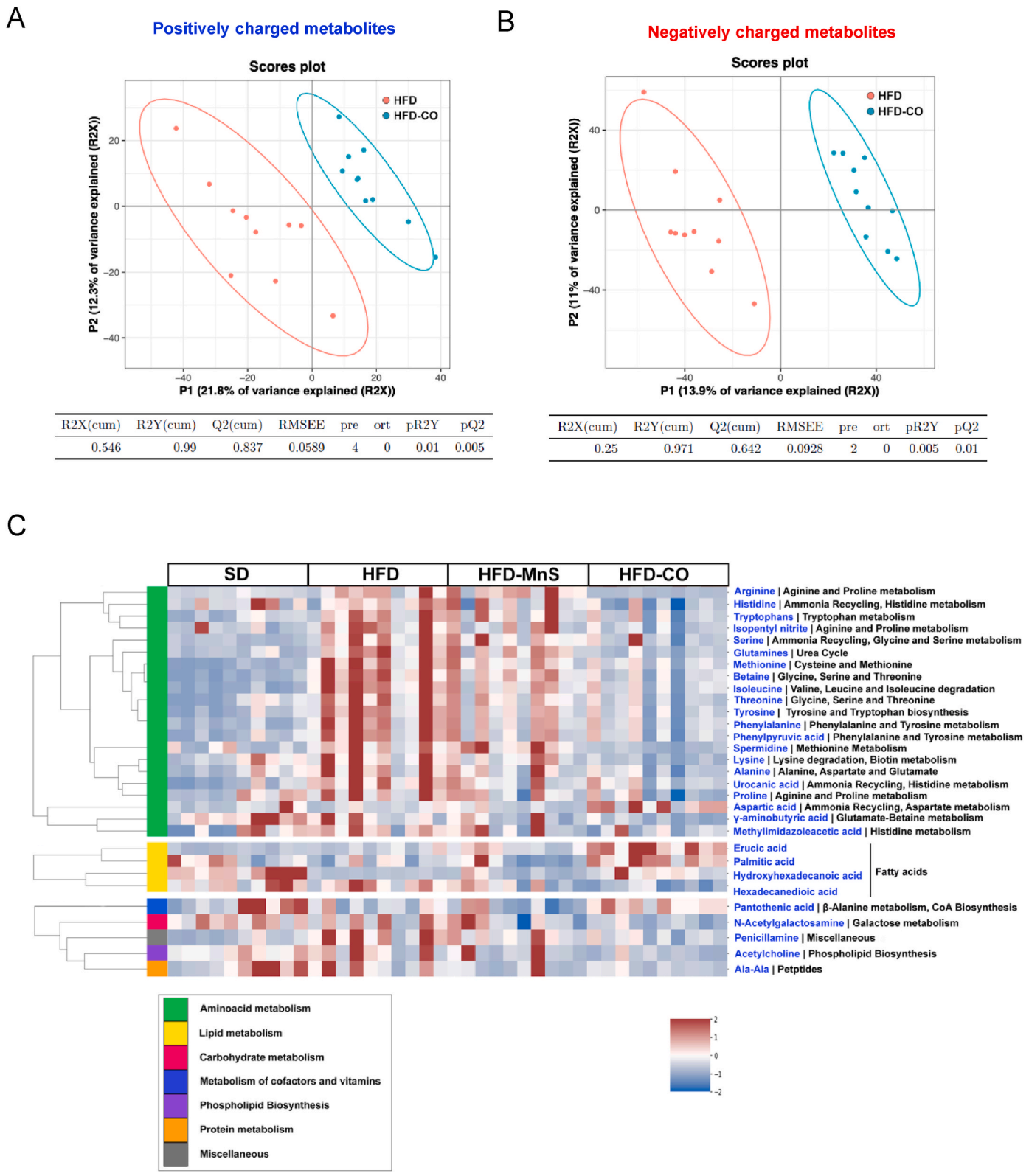

R2X(cum)	R2Y(cum)	Q2(cum)	RMSEE	pre	ort	pR2Y	pQ2
0.546	0.99	0.837	0.0589	4	0	0.01	0.005

R2X(cum)	R2Y(cum)	Q2(cum)	RMSEE	pre	ort	pR2Y	pQ2
0.25	0.971	0.642	0.0928	2	0	0.005	0.01

Fig. 5. Alterations of fecal metabolites induced by HFD are markedly reversed by treatment with CORM-401. Untargeted metabolomics analysis was used to detect fecal metabolites at week 14 in samples from mice fed a SD, HFD, HFD-MnS or HFD-CO. Partial least squares discriminant analysis (PLS-DA) score plots showing the distribution of positively (**A**) and negatively (**B**) charged fecal metabolites in HFD versus HFD-CO (n = 10). Parameters showing the goodness fit (pR2Y) and predictability of the model (pQ2) are shown underneath the plots. (**C**) Heatmap of the top 30 fecal metabolites significantly different between all groups. The name of the specific metabolite is in blue on the right hand side of the heatmap and the main metabolic pathways to which the metabolites belong are reported in different colors on the left of the heatmap. Significantly abundant metabolites ($P \leq 0.05$) between HFD and HFD-CO groups were selected using the Wilcoxon non-parametric test. (For interpretation of the references to color in this figure legend, the reader is referred to the Web version of this article.)

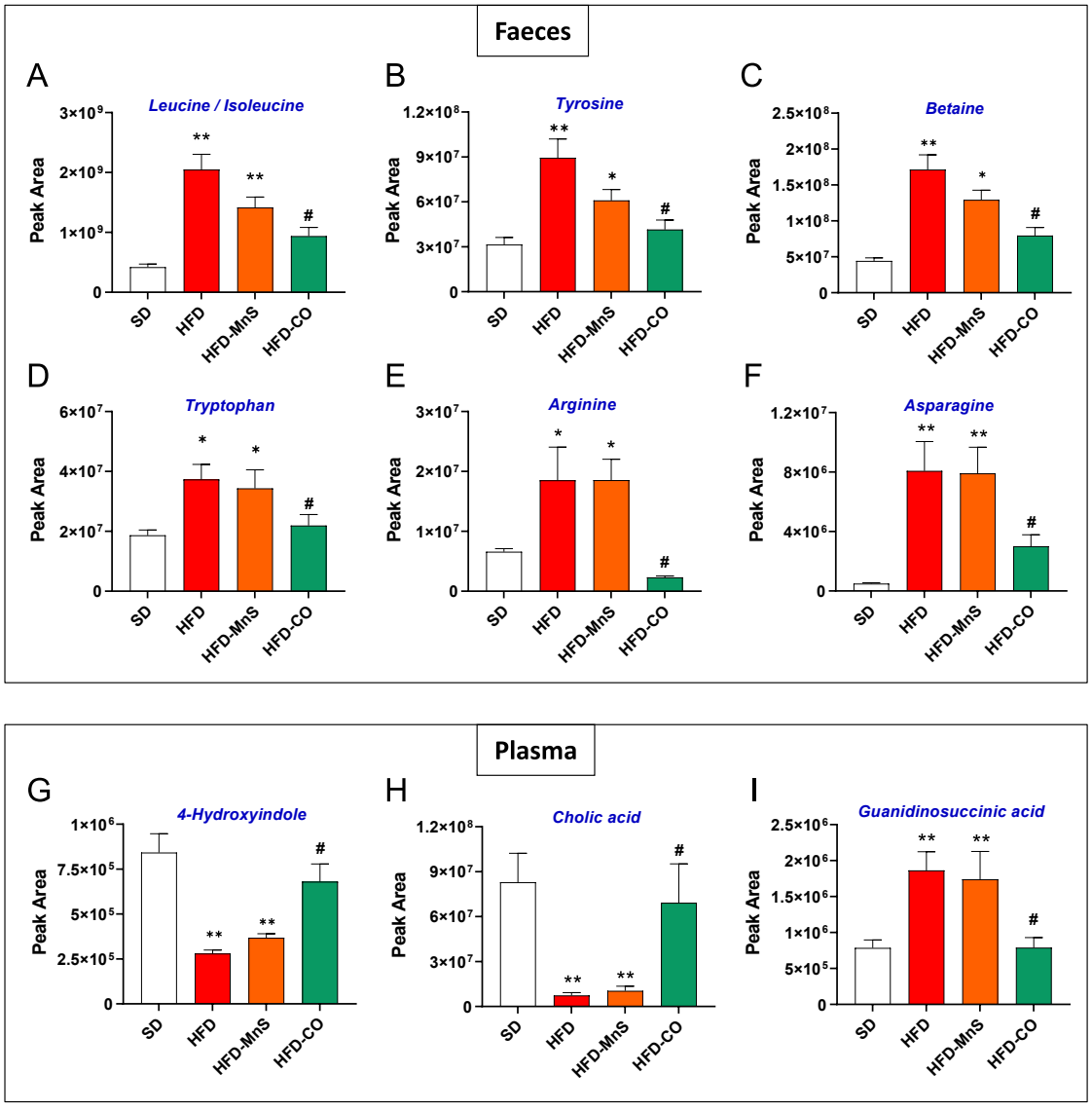

Fig. 6. CORM-401 normalizes the levels of key fecal amino acids and plasma tryptophan-derived bacterial metabolites altered by obesity. Untargeted metabolomics analysis was used to detect metabolites at week 14 in samples from mice fed a SD, HFD, HFD-MnS and HFD-CO (n = 10). (**A** to **F**) Levels of selected amino acids and derivatives in faeces expressed as relative peak areas. These amino acids were significantly increased by HFD and diminished to normal levels by CORM-401. (**G** to **I**) Levels of selected microbial metabolites in plasma from the same groups. It is shown that 4-hydroxindol and cholic acid were markedly decreased by HFD and restored to basal levels by CORM-401, while the uremic toxin guanidinosuccinic acid was increased by HFD and normalized by CORM-401. Data represent the mean ± SEM. $^{*}P < 0.05$, $^{**}P < 0.01$ vs. SD. $^{\#}P < 0.05$ vs. HFD group. One-way ANOVA with Bonferroni test for multiple comparisons between groups was used. (**J**) Relative abundance of the urea cycle pathway in bacteria, which was significantly increased by HFD and normalized by CORM-401 (n = 6). Box plots were analyzed by Wilcoxon non-parametric test. $^{*}P < 0.05$ and $^{**}P < 0.01$ between two groups. (**K**) The results show that the relative abundance of the microbiota *Oscillospiraceae* family from the *Firmicutes* phylum contributing to the urea cycle pathway is increased in HFD and normalized by CORM-401.

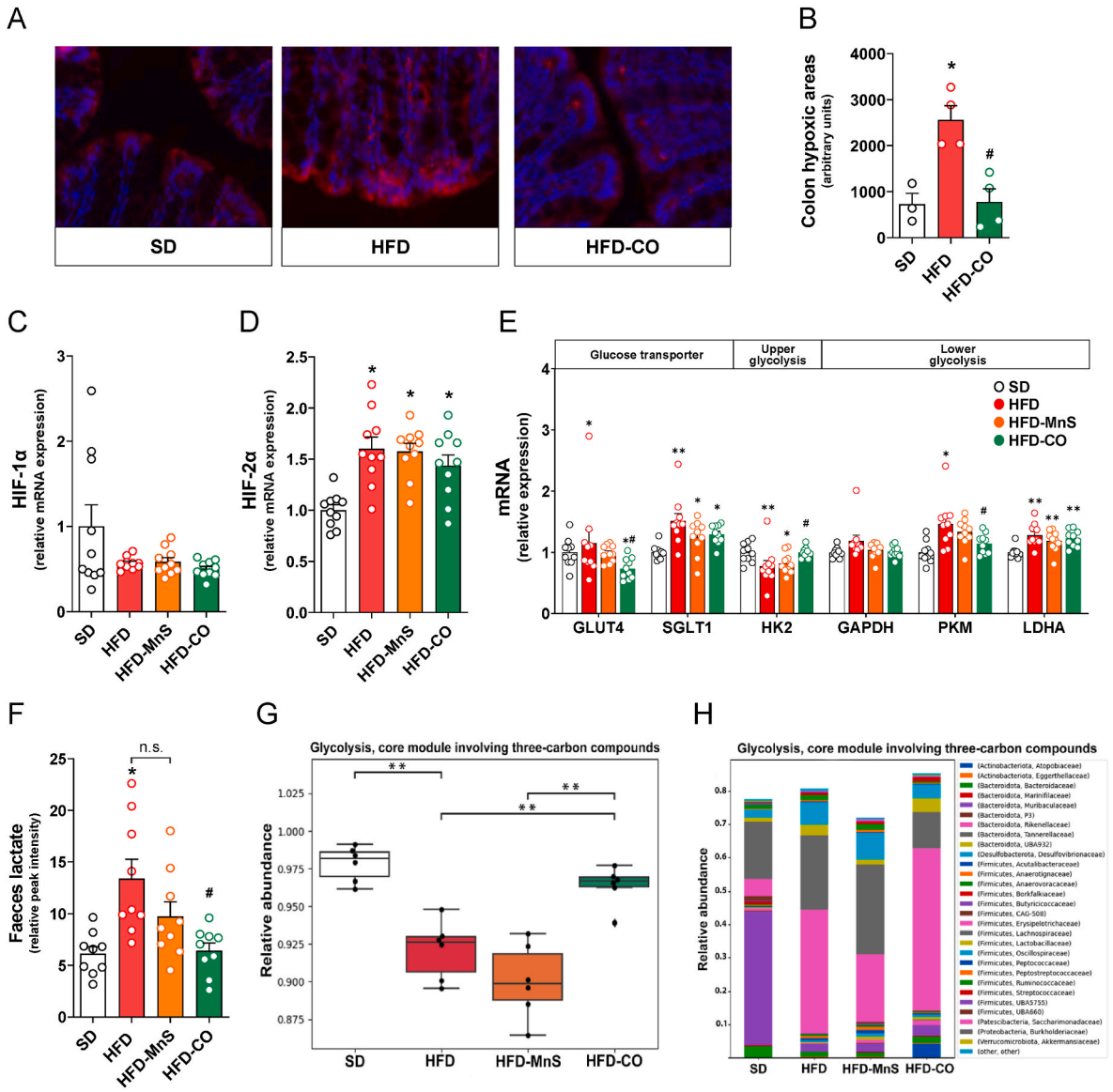

Fig. 7. CORM-401 reestablishes a normal hypoxic phenotype and glycolysis gene expression in the colon while restoring bacterial glycolysis in HFD-fed mice. (**A**) Representative images of colonic sections from mice under SD, HFD or HFD-CO stained with pimonidazole to visualize hypoxia at 14 weeks after treatments. (**B**) Quantification of colonic hypoxic areas calculated based on pimonidazole staining using ImageJ (n = 3–4). (**C** and **D**) HIF-1α and HIF-2α relative mRNA expression levels measured by RT-QPCR at week 14 in colon of mice fed a SD, HFD, HFD-MnS and HFD-CO (n = 10). (**E**) mRNA expression of glycolytic genes in the colon (n = 8–10). (**F**) Untargeted metabolomic profile of lactate in faeces collected at week 14 (n = 9–10). Data represent the mean ± SEM. $^{*}P < 0.05$, $^{**}P < 0.01$ vs. SD. $^{\#}P < 0.05$ vs. HFD group. One-way ANOVA with Bonferroni test for multiple comparisons between groups was used. (**G**) Relative abundance of the glycolysis pathway in bacteria, which was significantly decreased by HFD and normalized by CORM-401 (n = 6). Box plots were analyzed by Wilcoxon non parametric test. $^{**}P < 0.01$ between two groups. (**H**) The results show that several families contribute to the recovery of bacterial glycolysis in the HFD-CO group, with strong relative abundance of *Atopobiaceae* family from the *Actinobacteriota* phylum and *Erysipelotrichaceae* from the *Firmicutes* phylum.

suggest that these changes are dependent on a direct effect of CO on the gut tissue but derive also from a reshaping of microbiota composition by CORM-401.

5. Discussion

Obesity and weight gain are characterized by microbiota dysbiosis, and therapies restoring a healthy microbiome may be useful for the treatment of metabolic diseases. Recent results indicated that treating mice with low levels of CO counteracts HFD-induced weight gain and metabolic dysfunction [6,20,36]. Here we uncovered a novel role of CO, delivered to the mouse gut by oral administration with CORM-401, in reshaping the microbiota phenotype during obesity. We showed that CO enriched several known and unknown microbial species that were perturbed by HFD. Among many, the beneficial species *A. muciniphila* was strongly depleted by HFD and mostly enriched by CO. Analysis of bacterial transcripts revealed a restoration of microbial functional activity, with partial or full recovery of the citrate cycle, β-oxidation, respiratory chain and glycolysis. In addition, CO-treated mice exhibited normalization of several plasma and faecal metabolites that were disrupted by HFD, together with an amelioration of gut morphology, inflammatory profile and metabolic status. These findings provide a mechanistic insight and new perspectives for the therapeutic use of CORM-401 in obesity, identifying the microbiota as an important target for CO-mediated pharmacological action.

The HO-1/CO pathway protects against intestinal inflammation and plays an important role for the maintenance of gut homeostasis [37–40]. However, no previous studies investigated whether CO affects the gut

microbiota and whether this effect is beneficial for the host. Herein we demonstrate for the first time that prevention of HFD-induced obesity and metabolic imbalances by CO are coupled with profound changes in the composition of well-known and so far unidentified microbial species, suggesting their contribution to prevent weight gain and improve metabolism under HFD. Correlation analysis between body weight and abundance of bacterial species revealed that more than 20 species were significantly different between HFD and HFD-CO. Species that have been previously reported to be altered in obese humans and mice, such as *Roseburia* [41,42], *Acetatifactor* [43,44], *Adlercreutzia mucosi*cola [41] and *Lachnoclostridium* [45], were increased by HFD and normalized by CORM-401. An increased abundance of microbial species induced predominantly by CO was also striking. Notably, metagenomics and metatranscriptomics analysis as well as validation by PCR highlighted the strong enrichment of *A. muciniphila*, a species that was completely depleted by HFD but highly enriched by CO even above levels found in SD. *A. muciniphila* is a mucin-degrading bacterium that is inversely correlated with obesity and metabolic disorders in humans [46,47]. Because of its health benefits, *A. muciniphila* is currently tested as a probiotic and promising clinical trials are evaluating strategies to promote its abundance during obesity [13–15,48]. Thus, the decrease of crucial bacteria by HFD and the enhancement of species that have renowned salutary effects in the host appear to underlie the positive activity of CO during obesity.

Despite the fact that mice on SD and HFD-CO displayed a similar body weight and metabolic profile, the reshaping of the microbiota composition by CO led to a different population of bacteria compared to SD. However, CO restored fully or partially the functional signature of several bacterial pathways, including crucial core enzymes related to energy metabolism. Therefore, enhancement of the citrate cycle, increase in β-oxidation and cytochrome bd ubiquinol oxidase of the bacterial respiratory chain, normalization of coenzyme A and adenine ribonucleotide biosynthesis together with restoration of glycolysis by CO point to a much healthier microbial metabolic profile. It is surprising that mice on HFD and HFD-CO were eating the same regimen rich in fat and yet the microbiota from animals treated with CORM-401 could effectively fight HFD-induced metabolic disruption. Specific bacteria phyla, families and species uniquely contributed to the pathways modulated by CO, with the *Akkermansiaceae* family affecting mainly the citrate cycle and more than 1400 species contributing to the restoration of glycolysis. This latter case is very interesting, since the abundance of species supporting glycolysis was much higher in HFD-CO than SD. Therefore, CO stimulated alternative bacterial species to maintain glycolysis, highlighting the flexibility of different bacteria in engaging this fundamental metabolic pathway.

Our metabolomics analysis also revealed that amino acids and their products were accumulated in faeces of HFD mice but considerably reduced in HFD-CO. Of interest from a metabolic perspective are the BCAA, which levels are higher in obese individuals and are predictive markers of type 2 diabetes [31,49]. Since CO treatment ameliorated glucose tolerance and insulin resistance, the decreased BCAA levels induced by CORM-401 provides another explanation for the protective effect of CO. Higher amino acids levels in HFD were also accompanied by a significant rise in the urea cycle, showing that the build-up of amino acids in faeces was sensed by bacteria that responded by activating the pathway for elimination of ammonia from the amino group. Interestingly, accumulation of faecal amino acids in HFD mice was mirrored by the disappearance of amino acids and their metabolites from plasma, an effect that was again counteracted by CORM-401. Since HFD caused skeletal muscle atrophy, our data suggest that amino acids concentrate in faeces due to muscle degradation or because of an inability of this tissue to use them to synthesize proteins. This is particularly relevant for BCAA, which catabolism, occurring mainly in skeletal muscle [49], can be impaired during HFD by loss of muscle mass. Indeed, we observed that normalization of amino acids levels in faeces and plasma associated with normal appearance of muscle in HFD-CO. Of note, plasma levels of indole derivatives, a group of amino acid-derived metabolites generated by intestinal microbiota [50], were decreased by HFD and recovered by CORM-401. Conversely, faecal tryptophan levels were increased in mice on HFD and reduced to normal values by CO. Gut microbiota convert tryptophan to indoles that are absorbed by the host and are important mediators of the gut microbiome-host interaction [50]. Indoles contribute to maintaining gastrointestinal health, promoting the secretion of glucagon-like peptide 1 to delay gastric emptying and suppress appetite as well as improving insulin sensitivity [51]. Therefore, these data indicate that CO re-establishes the consumption of tryptophan by gut bacteria, resulting in the recovery of metabolically useful indoles. Interestingly, our network analysis using MicrobiomeAnalyst indicated that tryptophan metabolism was strongly linked to the enrichment of *A. muciniphila* in the HFD-CO group.

Obesity affects the microbiota and the gut tissue interacting with the microbiota. Indeed, the cecum and colon morphology and expression of inflammatory markers and genes controlling glycolysis were altered by HFD and mostly or partially normalized by CORM-401. In contrast to published studies [52], we observed that HFD induced a hypoxic state in the colon epithelium and that this effect was reversed by CO. However, as previously reported, we detected activation of HIF-2α by HFD [53]. Concomitantly, faecal lactate levels and expression of glucose transporter and lower glycolysis genes were enhanced in HFD, while the glycolysis pathway in bacteria was markedly decreased. We suggest that increased lactate levels in faeces by HFD are due to glycolytic metabolism in the host colon, and this lactate accumulation inhibits glycolysis in the microbial population and may contribute to microbial dysbiosis.

In this study we used CORM-401 and compared its effects to the negative control MnS. For the vast majority of the parameters assessed, CORM-401 was by far more efficacious than MnS, implicating CO accumulated in faeces and mouse tissues as the direct responsible for the overall improvement in body weight, insulin metabolism and reshaping the microbiota composition to a healthier phenotype during HFD. This is consistent with our previous published data on obesity, where we used another inactive compound in which CO was chemically depleted from CORM-401 [6]. Nevertheless, MnS exhibited some positive effects on selected parameters, suggesting that this part of CORM-401 can contribute to a minor extent to the beneficial properties exerted by this compound in obesity.

As obesity is a multifactorial pathological condition that affects several organs and tissues, our current data on CO-microbiota interaction and previous findings on the positive effects of CORM-401 on adipose tissue and metabolism [6,20] indicate the efficacy of CO to counteract a variety of dysfunctions elicited by HFD. With the present findings we uncover a new role for CO, indicating its potential use as a prebiotic to counteract microbiota dysbiosis arising during obesity and other disorders affecting the gastrointestinal tract. From a clinical perspective, toxicological studies will determine whether CORM-401 could be a useful and safe therapeutic to treat metabolic dysfunction.

CRediT authorship contribution statement

Djamal Eddine Benrahla: Writing – original draft, Supervision, Methodology, Investigation, Formal analysis, Data curation. **Shruti Mohan:** Investigation. **Matija Trickovic:** Validation, Software, Formal analysis. **Florence Anne Castelli:** Writing – review & editing, Validation, Methodology, Investigation. **Ghida Alloul:** Investigation. **Arielle Sobngwi:** Investigation. **Rosa Abdiche:** Investigation. **Silas Kieser:** Validation, Software, Methodology. **Vanessa Demontant:** Methodology, Investigation. **Elisabeth Trawinski:** Methodology, Investigation. **Céline Chollet:** Writing – review & editing, Validation, Methodology, Investigation. **Christophe Rodriguez:** Methodology, Investigation. **Hiroaki Kitagishi:** Writing – review & editing, Resources, Methodology. **François Fenaille:** Writing – review & editing, Validation, Methodology, Investigation. **Mirko Trajkovski:** Writing – review & editing,

Resources, Formal analysis, Data curation. **Roberto Motterlini:** Writing – review & editing, Writing – original draft, Validation, Supervision, Resources, Project administration, Methodology, Investigation, Funding acquisition, Formal analysis, Data curation, Conceptualization. **Roberta Foresti:** Writing – review & editing, Writing – original draft, Validation, Supervision, Resources, Project administration, Methodology, Investigation, Funding acquisition, Formal analysis, Data curation, Conceptualization.

Declaration of competing interest

R.M. and RF. are co-inventors on a patent application (EP4275682A1) submitted by INSERM and University Paris Val de Marne that covers therapeutic effects of carbon monoxide on dysbiosis.

Data availability

Data will be made available on request.

Acknowledgments

We thank the Histology, Genomic and EP3 platforms at the IMRB for their support during this project. R.F. and R.M. were funded by grants from the French Research Agency (ANR-15-RHUS-0003, ANR-18-CE18-0032, ANR-23-CE14-0080-01), the University of Paris Est Créteil (Pre-maturation Grant) and Erganeo Paris (CO-mBACT-AGE Grant). M. Trajkovski was funded by the Swiss National Science Foundation (SNSF) Project Grants (310030L_212267 and 310030_205042) and the European Research Council (ERC) Consolidator Grant (815962). D.E.B. was supported by a PhD fellowship from the Doctoral School, University of Paris Est Créteil.

Appendix A. Supplementary data

Supplementary data to this article can be found online at https://doi.org/10.1016/j.redox.2024.103153.

References

[1] R. Motterlini, R. Foresti, Heme oxygenase-1 as a target for drug discovery, Antioxidants Redox Signal. 20 (11) (2014) 1810–1826.
[2] R. Motterlini, R. Foresti, Biological signaling by carbon monoxide and carbon monoxide-releasing molecules (CO-RMs), Am. J. Physiol. Cell Physiol. 312 (3) (2017) C302–C313.
[3] H. Mosen, A. Salehi, P. Alm, R. Henningsson, J. Jimenez-Feltstrom, C.G. Ostenson, S. Efendic, I. Lundquist, Defective glucose-stimulated insulin release in the diabetic Goto-Kakizaki (GK) rat coincides with reduced activity of the islet carbon monoxide signaling pathway, Endocrinology 146 (3) (2005) 1553–1558.
[4] A. Jadhav, J.F. Ndisang, Treatment with heme arginate alleviates adipose tissue inflammation and improves insulin sensitivity and glucose metabolism in a rat model of Human primary aldosteronism, Free Radic. Biol. Med. 53 (12) (2012) 2277–2286.
[5] J.L. Wilson, F. Bouillaud, A.S. Almeida, H.L. Vieira, M.O. Ouidja, J.L. Dubois-Rande, R. Foresti, R. Motterlini, Carbon monoxide reverses the metabolic adaptation of microglia cells to an inflammatory stimulus, Free Rad, Biol. Med. 104 (2017) 311–323.
[6] L. Braud, M. Pini, L. Muchova, S. Manin, H. Kitagishi, D. Sawaki, G. Czibik, J. Ternacle, G. Derumeaux, R. Foresti, R. Motterlini, Carbon monoxide-induced metabolic switch in adipocytes improves insulin resistance in obese mice, JCI Insight 3 (22) (2018) e123485.
[7] N. Zmora, J. Suez, E. Elinav, You are what you eat: diet, health and the gut microbiota, Nat. Rev. Gastroenterol. Hepatol. 16 (1) (2019) 35–56.
[8] C.A. Thaiss, N. Zmora, M. Levy, E. Elinav, The microbiome and innate immunity, Nature 535 (7610) (2016) 65–74.
[9] E. Le Chatelier, T. Nielsen, J. Qin, E. Prifti, F. Hildebrand, G. Falony, M. Almeida, M. Arumugam, J.M. Batto, S. Kennedy, P. Leonard, J. Li, K. Burgdorf, N. Grarup, T. Jorgensen, I. Brandslund, H.B. Nielsen, A.S. Juncker, M. Bertalan, F. Levenez, N. Pons, S. Rasmussen, S. Sunagawa, J. Tap, S. Tims, E.G. Zoetendal, S. Brunak, K. Clement, J. Dore, M. Kleerebezem, K. Kristiansen, P. Renault, T. Sicheritz-Ponten, W.M. de Vos, J.D. Zucker, J. Raes, T. Hansen, P. Bork, J. Wang, S. D. Ehrlich, O. Pedersen, Richness of human gut microbiome correlates with metabolic markers, Nature 500 (7464) (2013) 541–546.
[10] R.E. Ley, F. Backhed, P. Turnbaugh, C.A. Lozupone, R.D. Knight, J.I. Gordon, Obesity alters gut microbial ecology, Proc. Natl. Acad. Sci. U. S. A 102 (31) (2005) 11070–11075.
[11] P.J. Turnbaugh, R.E. Ley, M.A. Mahowald, V. Magrini, E.R. Mardis, J.I. Gordon, An obesity-associated gut microbiome with increased capacity for energy harvest, Nature 444 (7122) (2006) 1027–1031.
[12] A. Everard, C. Belzer, L. Geurts, J.P. Ouwerkerk, C. Druart, L.B. Bindels, Y. Guiot, M. Derrien, G.G. Muccioli, N.M. Delzenne, W.M. de Vos, P.D. Cani, Cross-talk between Akkermansia muciniphila and intestinal epithelium controls diet-induced obesity, Proc. Natl. Acad. Sci. U. S. A 110 (22) (2013) 9066–9071.
[13] C. Depommier, H.M. Van, A. Everard, N.M. Delzenne, W.M. de Vos, P.D. Cani, Pasteurized Akkermansia muciniphila increases whole-body energy expenditure and fecal energy excretion in diet-induced obese mice, Gut Microb. 11 (5) (2020) 1231–1245.
[14] C. Depommier, A. Everard, C. Druart, H. Plovier, M. Van Hul, S. Vieira-Silva, G. Falony, J. Raes, D. Maiter, N.M. Delzenne, M. de Barsy, A. Loumaye, M. P. Hermans, J.P. Thissen, W.M. de Vos, P.D. Cani, Supplementation with Akkermansia muciniphila in overweight and obese human volunteers: a proof-of-concept exploratory study, Nat. Med. 25 (7) (2019) 1096–1103.
[15] P.D. Cani, C. Depommier, M. Derrien, A. Everard, W.M. de Vos, Akkermansia muciniphila: paradigm for next-generation beneficial microorganisms, Nat. Rev. Gastroenterol. Hepatol. 19 (10) (2022) 625–637.
[16] S.H. Crook, B.E. Mann, J.A.H.M. Meijer, H. Adams, P. Sawle, D. Scapens, R. Motterlini, [Mn(CO)4{S2CNMe(CH2CO2H)}], a new water-soluble CO-releasing molecule, Dalton Trans. 40 (16) (2011) 4230–4235.
[17] A. Ollivier, R. Foresti, Z. El Ali, T. Martens, H. Kitagishi, R. Motterlini, M. Rivard, Design and biological evaluation of manganese- and ruthenium-based hybrid CO-releasing molecules (HYCOs), ChemMedChem 14 (2019) 1684–1691.
[18] H. Kitagishi, S. Negi, A. Kiriyama, A. Honbo, Y. Sugiura, A.T. Kawaguchi, K. Kano, A diatomic molecule receptor that removes CO in a living organism, Angew. Chem., Int. Ed. Engl. 49 (7) (2010) 1312–1315.
[19] Q. Mao, A.T. Kawaguchi, S. Mizobata, R. Motterlini, R. Foresti, H. Kitagishi, Sensitive quantification of carbon monoxide (CO) *in vivo* reveals a protective role of circulating hemoglobin in CO intoxication, Commun, Biol. 4 (2021) 425, https://doi.org/10.1038/s42003-021-01880-1.
[20] S. Mohan, L.A. Barel, D.E. Benrahla, B. Do, Q. Mao, H. Kitagishi, M. Rivard, R. Motterlini, R. Foresti, Development of carbon monoxide-releasing molecules conjugated to polysaccharides (glyco-CORMs) for delivering CO during obesity, Pharmacol. Res. 191 (2023) 106770, https://doi.org/10.1016/j.phrs.2023.
[21] F.L. Rodkey, T.A. Hill, L.L. Pitts, R.F. Robertson, Spectrophotometric measurement of carboxyhemoglobin and methemoglobin in blood, Clin. Chem. 25 (8) (1979) 1388–1393.
[22] A. Nikam, A. Ollivier, M. Rivard, J.L. Wilson, K. Mebarki, T. Martens, J.L. Dubois-Rande, R. Motterlini, R. Foresti, Diverse Nrf2 activators coordinated to cobalt carbonyls induce heme oxygenase-1 and release carbon monoxide in vitro and in vivo, J. Med. Chem. 59 (2) (2016) 756–762.
[23] M. Tabone, C. Bressa, J.A. Garcia-Merino, D. Moreno-Perez, E.C. Van, F.A. Castelli, F. Fenaille, M. Larrosa, The effect of acute moderate-intensity exercise on the serum and fecal metabolomes and the gut microbiota of cross-country endurance athletes, Sci. Rep. 11 (1) (2021) 3558.
[24] S. Boudah, M.F. Olivier, S. Aros-Calt, L. Oliveira, F. Fenaille, J.C. Tabet, C. Junot, Annotation of the human serum metabolome by coupling three liquid chromatography methods to high-resolution mass spectrometry, J. Chromatogr., B: Anal. Technol. Biomed. Life Sci. 966 (2014) 34–47.
[25] S. Minegishi, A. Yumura, H. Miyoshi, S. Negi, S. Taketani, R. Motterlini, R. Foresti, K. Kano, H. Kitagishi, Detection and removal of endogenous carbon monoxide by selective and cell permeable hemoprotein-model complexes, J. Am. Chem. Soc. 139 (16) (2017) 5984–5991.
[26] B.W. Parks, E. Nam, E. Org, E. Kostem, F. Norheim, S.T. Hui, C. Pan, M. Civelek, C. D. Rau, B.J. Bennett, M. Mehrabian, L.K. Ursell, A. He, L.W. Castellani, B. Zinker, M. Kirby, T.A. Drake, C.A. Drevon, R. Knight, P. Gargalovic, T. Kirchgessner, E. Eskin, A.J. Lusis, Genetic control of obesity and gut microbiota composition in response to high-fat, high-sucrose diet in mice, Cell Metabol. 17 (1) (2013) 141–152.
[27] S. Kieser, E.M. Zdobnov, M. Trajkovski, Comprehensive mouse microbiota genome catalog reveals major difference to its human counterpart, PLoS Comput. Biol. 18 (3) (2022) e1009947.
[28] S. Kieser, J. Brown, E.M. Zdobnov, M. Trajkovski, L.A. McCue, ATLAS: a Snakemake workflow for assembly, annotation, and genomic binning of metagenome sequence data, BMC Bioinf. 21 (1) (2020) 257.
[29] T. Vasanthakumar, J.L. Rubinstein, Structure and roles of V-type ATPases, Trends Biochem. Sci. 45 (4) (2020) 295–307.
[30] O. Geiger, I.M. Lopez-Lara, C. Sohlenkamp, Phosphatidylcholine biosynthesis and function in bacteria, Biochim. Biophys. Acta 1831 (3) (2013) 503–513.
[31] C.B. Newgard, J. An, J.R. Bain, M.J. Muehlbauer, R.D. Stevens, L.F. Lien, A. M. Haqq, S.H. Shah, M. Arlotto, C.A. Slentz, J. Rochon, D. Gallup, O. Ilkayeva, B. R. Wenner, W.S. Yancy Jr., H. Eisenson, G. Musante, R.S. Surwit, D.S. Millington, M.D. Butler, L.P. Svetkey, A branched-chain amino acid-related metabolic signature that differentiates obese and lean humans and contributes to insulin resistance, Cell Metabol. 9 (4) (2009) 311–326.
[32] C. Hellmuth, F.F. Kirchberg, N. Lass, U. Harder, W. Peissner, B. Koletzko, T. Reinehr, Tyrosine is associated with insulin resistance in longitudinal metabolomic profiling of obese children, J. Diabetes Res. (2016 2016) 2108909.
[33] A. Molinaro, A. Wahlstrom, H.U. Marschall, Role of bile acids in metabolic control, trends Endocrinol, Meta 29 (1) (2018) 31–41.

[34] S.K. Nigam, K.T. Bush, Uraemic syndrome of chronic kidney disease: altered remote sensing and signalling, Nat. Rev. Nephrol. 15 (5) (2019) 301–316.
[35] E. Mishima, S. Fukuda, C. Mukawa, A. Yuri, Y. Kanemitsu, Y. Matsumoto, Y. Akiyama, N.N. Fukuda, H. Tsukamoto, K. Asaji, H. Shima, K. Kikuchi, C. Suzuki, T. Suzuki, Y. Tomioka, T. Soga, S. Ito, T. Abe, Evaluation of the impact of gut microbiota on uremic solute accumulation by a CE-TOFMS-based metabolomics approach, Kidney Int. 92 (3) (2017) 634–645.
[36] P.A. Hosick, A.A. Alamodi, M.V. Storm, M.U. Gousset, B.E. Pruett, W. Gray III, J. Stout, D.E. Stec, Chronic carbon monoxide treatment attenuates development of obesity and remodels adipocytes in mice fed a high-fat diet, Int. J. Obes. 38 (1) (2014) 132–139.
[37] J.C. Onyiah, S.Z. Sheikh, N. Maharshak, L.E. Otterbein, S.E. Plevy, Heme oxygenase-1 and carbon monoxide regulate intestinal homeostasis and mucosal immune responses to the enteric microbiota, Gut Microb. 5 (2) (2014) 220–224.
[38] J.C. Onyiah, S.Z. Sheikh, N. Maharshak, E.C. Steinbach, S.M. Russo, T. Kobayashi, L.C. Mackey, J.J. Hansen, A.J. Moeser, J.F. Rawls, L.B. Borst, L.E. Otterbein, S. E. Plevy, Carbon monoxide and heme oxygenase-1 prevent intestinal inflammation in mice by promoting bacterial clearance, Gastroenterology 144 (4) (2013) 789–798.
[39] R.A. Hegazi, K.N. Rao, A. Mayle, A.R. Sepulveda, L.E. Otterbein, S.E. Plevy, Carbon monoxide ameliorates chronic murine colitis through a heme oxygenase 1-dependent pathway, J. Exp. Med. 202 (12) (2005) 1703–1713.
[40] D. Babu, G. Leclercq, V. Goossens, Q. Remijsen, P. Vandenabeele, R. Motterlini, R. A. Lefebvre, Antioxidant potential of CORM-A1 and resveratrol during TNF-alpha/cycloheximide-induced oxidative stress and apoptosis in murine intestinal epithelial MODE-K cells, Toxicol. Appl. Pharmacol. 288 (2015) 161–178.
[41] Nitert M. Dekker, A. Mousa, H.L. Barrett, N. Naderpoor, de Court, Altered gut microbiota composition is associated with Back Pain in overweight and obese individuals, Front. Endocrinol. 11 (2020) 605.
[42] Z. Xu, W. Jiang, W. Huang, Y. Lin, F.K.L. Chan, S.C. Ng, Gut microbiota in patients with obesity and metabolic disorders - a systematic review, Genes Nutr 17 (1) (2022) 2.
[43] D. Wang, L. Wang, L. Han, B. Wang, R. Shi, J. Ye, B. Xia, Z. Zhao, B. Zhao, X. Liu, Leucine-restricted diet ameliorates obesity-linked cognitive Deficits: involvement of the microbiota-gut-brain Axis, J. Agric. Food Chem. 71 (24) (2023) 9404–9418.
[44] X. Wang, C. Yu, X. Liu, J. Yang, Y. Feng, Y. Wu, Y. Xu, Y. Zhu, W. Li, Fenofibrate ameliorated systemic and retinal inflammation and modulated gut microbiota in high-fat diet-induced mice, Front. Cell. Infect. Microbiol. 12 (2022) 839592.
[45] J. Gong, Y. Shen, H. Zhang, M. Cao, M. Guo, J. He, B. Zhang, C. Xiao, Gut microbiota Characteristics of People with obesity by meta-analysis of existing datasets, Nutrients 14 (14) (2022) 2993.
[46] M.C. Dao, A. Everard, J. Aron-Wisnewsky, N. Sokolovska, E. Prifti, E.O. Verger, B. D. Kayser, F. Levenez, J. Chilloux, L. Hoyles, M.E. Dumas, S.W. Rizkalla, J. Dore, P. D. Cani, K. Clement, Akkermansia muciniphila and improved metabolic health during a dietary intervention in obesity: relationship with gut microbiome richness and ecology, Gut 65 (3) (2016) 426–436.
[47] M. Schneeberger, A. Everard, A.G. Gomez-Valades, S. Matamoros, S. Ramirez, N. M. Delzenne, R. Gomis, M. Claret, P.D. Cani, Akkermansia muciniphila inversely correlates with the onset of inflammation, altered adipose tissue metabolism and metabolic disorders during obesity in mice, Sci. Rep. 5 (2015) 16643.
[48] P.D. Cani, W.M. de Vos, Next-generation beneficial Microbes: the case of Akkermansia muciniphila, Front. Microbiol. 8 (2017) 1765.
[49] F. Bifari, E. Nisoli, Branched-chain amino acids differently modulate catabolic and anabolic states in mammals: a pharmacological point of view, Br. J. Pharmacol. 174 (11) (2017) 1366–1377.
[50] A. Agus, J. Planchais, H. Sokol, Gut microbiota regulation of tryptophan metabolism in health and disease, cell host, Microbe 23 (6) (2018) 716–724.
[51] X. Ye, H. Li, K. Anjum, X. Zhong, S. Miao, G. Zheng, W. Liu, L. Li, Dual role of indoles derived from intestinal microbiota on human health, Front. Immunol. 13 (2022) 903526.
[52] W. Yoo, J.K. Zieba, N.J. Foegeding, T.P. Torres, C.D. Shelton, N.G. Shealy, A. J. Byndloss, S.A. Cevallos, E. Gertz, C.R. Tiffany, J.D. Thomas, Y. Litvak, H. Nguyen, E.E. Olsan, B.J. Bennett, J.C. Rathmell, A.S. Major, A.J. Baumler, M. X. Byndloss, High-fat diet-induced colonocyte dysfunction escalates microbiota-derived trimethylamine N-oxide, Science 373 (6556) (2021) 813–818.
[53] C. Xie, T. Yagai, Y. Luo, X. Liang, T. Chen, Q. Wang, D. Sun, J. Zhao, S. K. Ramakrishnan, L. Sun, C. Jiang, X. Xue, Y. Tian, K.W. Krausz, A.D. Patterson, Y. M. Shah, Y. Wu, C. Jiang, F.J. Gonzalez, Activation of intestinal hypoxia-inducible factor 2alpha during obesity contributes to hepatic steatosis, Nat. Med. 23 (11) (2017) 1298–1308.